Phys Chem Minerals
DOI 10.1007/s00269-009-0303-5

ORIGINAL PAPER

# Deformation of lower-mantle ferropericlase (Mg,Fe)O across the electronic spin transition

**Jung-Fu Lin · Hans-Rudolf Wenk · Marco Voltolini · Sergio Speziale · Jinfu Shu · Thomas S. Duffy**

Received: 8 January 2009 / Accepted: 31 March 2009


**Abstract** Recent high-pressure studies have shown that an electronic spin transition of iron in ferropericlase, an expected major phase of Earth's lower mantle, results in changes in its properties, including density, incompressibility, radiative thermal conductivity, electrical conductivity, and sound velocities. To understand the rheology of ferropericlase across the spin transition, we have used in situ radial X-ray diffraction techniques to examine ferropericlase, $(Mg_{0.83},Fe_{0.17})O$, deformed non-hydrostatically in a diamond cell up to 81 GPa at room temperature. Compared with recent quasi-hydrostatic studies, the range of the spin transition is shifted by approximately 20 GPa as a result of the presence of large differential stress in the sample. We also observed a reduction in incompressibility and in the unit cell volume of 3% across the spin transition. Our radial X-ray diffraction results show that the {0 0 1} texture is the dominant lattice preferred orientation in ferropericlase across the spin transition and in the low-spin state. Viscoplastic self-consistent polycrystal plasticity simulations suggest that this preferred orientation pattern is produced by {1 1 0}<1–10> slip. Analyzing our radial X-ray diffraction patterns using lattice strain theory, we evaluated the lattice *d*-spacings of ferropericlase and Mo as a function of the $\psi$ angle between the compression direction and the diffracting plane normal. These analyses give the ratio between the uniaxial stress component ($t$) and the shear modulus ($G$) under constant stress condition, which represents a proxy for the supported differential stress and elastic strength. This ratio in the mixed-spin and low-spin states is lower than what is expected from previous studies of high-spin ferropericlase, indicating that the spin transition results in a reduced differential stress and elastic strength along with the volume reduction. The influence of the spin transition on the differential stress and strength of ferropericlase is expected to be less dominant across the wide spin transition zone at high pressure–temperature conditions relevant to the lower mantle.

**Keywords** Ferropericlase · Spin transition · Lower mantle · Deformation · Radial X-ray diffraction

J.-F. Lin (✉)
Department of Geological Sciences,
Jackson School of Geosciences,
The University of Texas at Austin,
Austin, TX 78712, USA
e-mail: afu@jsg.utexas.edu

H.-R. Wenk · M. Voltolini
Department of Earth and Planetary Science,
University of California, Berkeley, CA 94720, USA

S. Speziale
GeoForschungsZentrum Potsdam, Telegrafenberg,
14473 Potsdam, Germany

J. Shu
Geophysical Laboratory, Carnegie Institution of Washington,
Washington, DC 20015, USA

T. S. Duffy
Department of Geosciences, Princeton University,
Princeton, NJ 08544, USA

## Introduction

Earth's lower mantle is believed to consist of approximately one-third ferropericlase [(Mg,Fe)O] and two-thirds aluminous silicate perovskite [Al-$(Mg,Fe)SiO_3$], together with a few percent of calcium silicate perovskite ($CaSiO_3$), based on a pyrolytic compositional model (Ringwood 1982). The lattice preferred orientation and elastic

Published online: 21 April 2009

anisotropy of this mineral assemblage are thus predominantly responsible for the development of the lower mantle deformation and the origin of the seismic anisotropy (e.g., Karato 1998; Stretton et al. 2001; McNamara et al. 2002; Merkel et al. 2002; Yamazaki and Karato 2002; Heidelbach et al. 2003; Long et al. 2006; Tommaseo et al. 2006; Wenk et al. 2006). Therefore, studying the lattice preferred orientation, plastic flow and flow-induced fabrics in ferropericlase, perovskite, and post-perovskite is of great importance to understanding geophysics and geodynamics of the lower mantle. Although ferropericlase constitutes only approximately one-third of this region by volume, it exhibits weaker creep strength and higher elastic anisotropy than the more abundant perovskite and perhaps post-perovskite, and likely plays important roles in the deformation of the lower mantle. Recent texture studies of pure MgO and high-spin ferropericlase at high pressures indicate that the {1 1 0}<1–10> slip system (i.e., slip on the planes {1 1 0} in the <110> directions), dominates at room temperature (Merkel et al. 2002; Tommaseo et al. 2006; Wenk et al. 2006), whereas at higher temperature slip on {1 0 0} and {1 1 0} planes in the <1 1 0> direction becomes equally active (e.g., Stretton et al. 2001). These studies have all been performed on high-spin ferropericlase or pure MgO and therefore may not reflect the properties of ferropericlase in the mixed-spin and low-spin states under lower mantle conditions.

Electronic spin-pairing transitions of iron have been recently reported to occur in lower-mantle ferropericlase, perovskite, and post-perovskite at high pressures and/or high temperatures (e.g., Badro et al. 2003; Sturhahn et al. 2005; Persson et al. 2006; Tsuchiya et al. 2006; Fei et al. 2007; Lin et al. 2005, 2007a, 2008; McCammon et al. 2008). These studies indicate that the high-spin to low-spin transition of iron in ferropericlase occurs at approximately 40–50 GPa and room temperature (i.e., see Lin and Tsuchiya 2008 for a recent review). At the lower mantle pressure–temperature conditions, a wide spin transition zone (STZ) in ferropericlase may occur from approximately 1,000 km in depth to 2,200 km, i.e., from the top to the bottom of the lower mantle (Lin et al. 2007a). Furthermore, the spin transition of iron results in increased density and incompressibility, and reduced radiative thermal conductivity and electrical conductivity from the high-spin to the low-spin ferropericlase (Goncharov et al. 2006; Fei et al. 2007; Keppler et al. 2007; Lin et al. 2005, 2006b, 2007b, 2008; Crowhurst et al. 2008). In addition, a reduction in sound velocities and elastic moduli of ferropericlase with 6% FeO within the transition has been recently reported, though its elastic anisotropy factor remains high through the transition (Crowhurst et al. 2008). To understand the effects of the spin transition on the deformation of ferropericlase under lower mantle pressures, we have carried out in situ radial X-ray diffraction (RXD) of ferropericlase deformed non-hydrostatically across the spin transition in a diamond anvil cell (DAC) up to 81 GPa. We analyze the texture, differential stress, and strength of ferropericlase in the high-spin, mixed-spin, and low-spin states, and discuss the influence of the spin transition on the deformation of ferropericlase.

## Experimental method

A beryllium gasket was pre-indented to a thickness of 25 μm using a panoramic DAC with a pair of beveled diamonds with 150-μm inner culets and 300-μm outer culets. A hole of 40 μm was drilled in the pre-indented gasket and used as the sample chamber (Fig. 1). A small flake of polycrystalline Mo, approximately 15 μm in diameter and 2 μm in thickness, was placed into the sample chamber and used as the pressure calibrant and X-ray marker. Polycrystalline ferropericlase [$(Mg_{0.83},Fe_{0.17})O$] sample was then loaded into the sample chamber and compressed under non-hydrostatic conditions. The polycrystalline $(Mg_{0.83},Fe_{0.17})O$ sample was synthesized by sintering stoichiometric mixtures of MgO and Fe powder under a controlled $CO_2$–CO atmosphere near the iron-wüstite buffer (Lin et al. 2005). The ferric iron ($Fe^{3+}$) content of the samples was below the detection limit of Mössbauer spectroscopy and magnetite ($Fe_3O_4$) was not detected in the X-ray diffraction pattern.

High-pressure RXD experiments in a DAC were conducted using energy-dispersive synchrotron X-ray diffraction at beamline X17C of the National Synchrotron Light Source (NSLS) at Brookhaven National Laboratory (BNL).

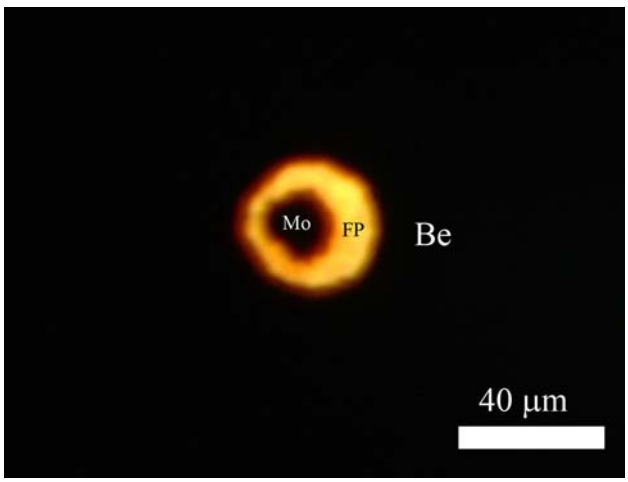


**Fig. 1** Image of the ferropericlase [$(Mg_{0.83},Fe_{0.17})O$] sample taken in transmitted light in a DAC at ~16 GPa. A small flake of polycrystalline Mo was used as the pressure calibrant and X-ray marker. Be gasket was used to contain the sample and Mo at high pressures

A polychromatic incident X-ray beam with energy range of approximately 22–70 keV was focused to approximately 10 μm in diameter (full width at half maximum (FWHM)) at the sample position, and a set of cleanup slits was used to reduce the tails of the focused X-ray beam. X-ray fluorescence and absorption of Mo were used to align the sample chamber with the incident X-rays. The incident X-ray beam passed radially through the Be gasket perpendicular to the compression axis of the DAC. RXD patterns of ferropericlase [$(Mg_{0.83},Fe_{0.17})O$] and Mo were detected between 16 GPa and 81 GPa by a Ge solid-state detector at a $2\theta$ of 12° (Fig. 2) (Singh et al. 1998). At each pressure, RXD patterns were collected as a function of the angle ($\psi$) between the diffracting plane normal and the stress axis of the DAC at angular intervals of approximately 10°–15° for about 20–30 min each. The $\psi$ angle is defined as 0° when the diffracting plane normal is parallel to the stress axis of the DAC, and 90° when the diffracting plane normal is perpendicular to the stress axis.

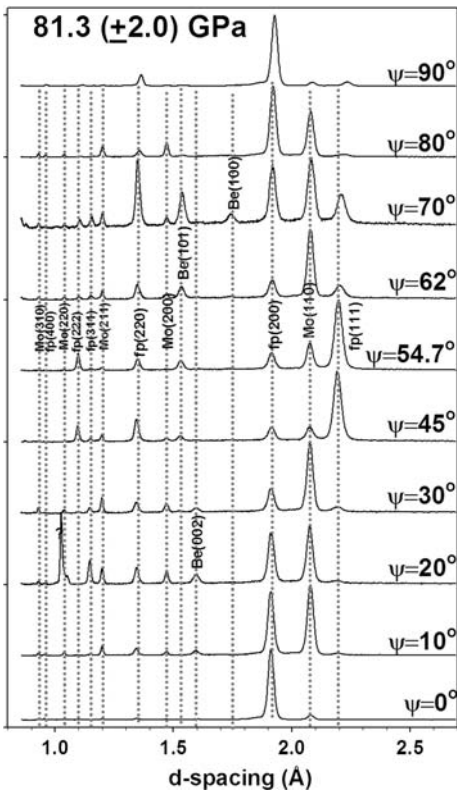


**Fig. 2** Representative RXD patterns of ferropericlase [$(Mg_{0.83},Fe_{0.17})O$] at 81.3 (±2.0) GPa as a function of the $\psi$ angle. *fp* ferropericlase; *Mo* molybdenum pressure marker. Errors on pressures are calculated from the standard deviation of the *d*-spacings of Mo. Ferropericlase remains in the cubic rock-salt structure under non-hydrostatic condition up to 81 GPa. The strong intensity variations in ferropericlase with $\psi$ immediately indicate preferred orientation. For example, the intensity of the 1 1 1 diffraction line of ferropericlase is almost zero at $\psi = 0^\circ$ and has a maximum at $\psi = 54.7^\circ$. Also Mo is strongly textured. These spectra, over a *d*-spacing range from 1.0 to 2.5 Å that includes six diffraction lines of ferropericlase, were used for analyzing the texture, *EoS*, differential stress, and strength of ferropericlase across the spin transition

The *d*-spacings of the X-ray diffraction peaks were obtained by fitting Voigt line shapes to the diffraction spectra after background subtraction. For Mo, five diffraction lines (110, 200, 211, 220, and 310) were used for the analyses, while six diffraction lines of ferropericlase (111, 200, 220, 311, 222, and 400) were used. The corresponding equivalent hydrostatic pressures were determined from the lattice parameters of Mo obtained from the measured *d*-spacings at $\psi$ of 54.7° (Singh et al. 1998; Duffy et al. 1999), using the equation of state (EoS) of Mo by Hixson and Fritz (1992). Errors on pressures were calculated from the standard variation of the *d*-spacings of Mo.

## Results

Seven sets of the RXD patterns of polycrystalline ferropericlase [$(Mg_{0.83},Fe_{0.17})O$] and Mo have been collected at 16.5, 45.2, 51.6, 56.6, 62.5, 68.4, and 81.3 GPa as a function of the $\psi$ angle. The unit cell volumes of ferropericlase were calculated using the radial X-ray diffraction patterns at the $\psi$ angle of 54.7° where the compression condition was equivalent to hydrostatic based on the lattice strain theory (Fig. 3) (Singh et al. 1998). The unit cell volumes of ferropericlase at the $\psi$ angle of 54.7° are systematically higher than those under quasi-hydrostatic conditions between 45 and 68 GPa, but become consistent with those of low-spin ferropericlase and pure MgO at 81 GPa (Fig. 3, 4) (Speziale et al. 2001; Lin et al. 2005; Fei et al. 2007), indicating the occurrence of the mixed-spin states between 45 and 68 GPa and the low-spin state at 81 GPa.

We used the Rietveld method that relies on the full diffraction spectrum and applied the E-WIMV texture algorithm in the Rietveld code MAUD to calculate orientation distributions (Lutterotti et al. 1997). The orientation distributions were then exported, smoothed, and used in the Beartex code (Wenk et al. 1998) to calculate inverse pole figures that represent the probability of finding crystal directions parallel to the compression direction in ferropericlase (Fig. 5). A moderate texture develops at 16 GPa and strengthens with increasing pressure. All inverse pole figures above 45 GPa show a main maximum at 0 0 1, with a subsidiary 0 1 1 maximum developing. These texture patterns are consistent with predominantly {1 1 0}<1–10> slip (e.g., Stretton et al. 2001; Merkel et al. 2002; Tommaseo et al. 2006), and the slip systems do not change across the spin transition in ferropericlase (Fig. 5).

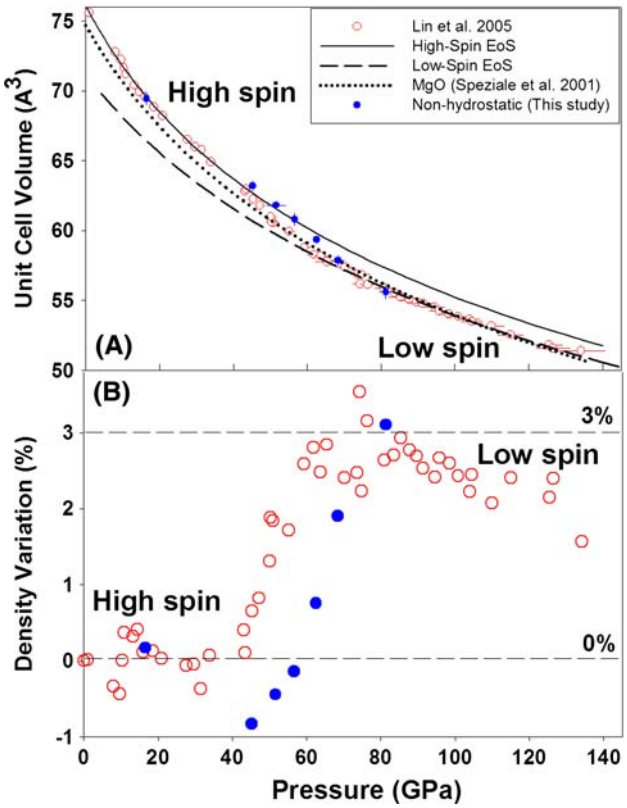


**Fig. 3** Unit cell volume (**a**) and volume difference (**b**) of $(Mg_{0.83},Fe_{0.17})O$ across the spin transition. Our non-hydrostatic results (*blue solid symbols*) are compared with a previous study under quasi-hydrostatic condition using Ne pressure medium (*red open symbols*) (Lin et al. 2005)

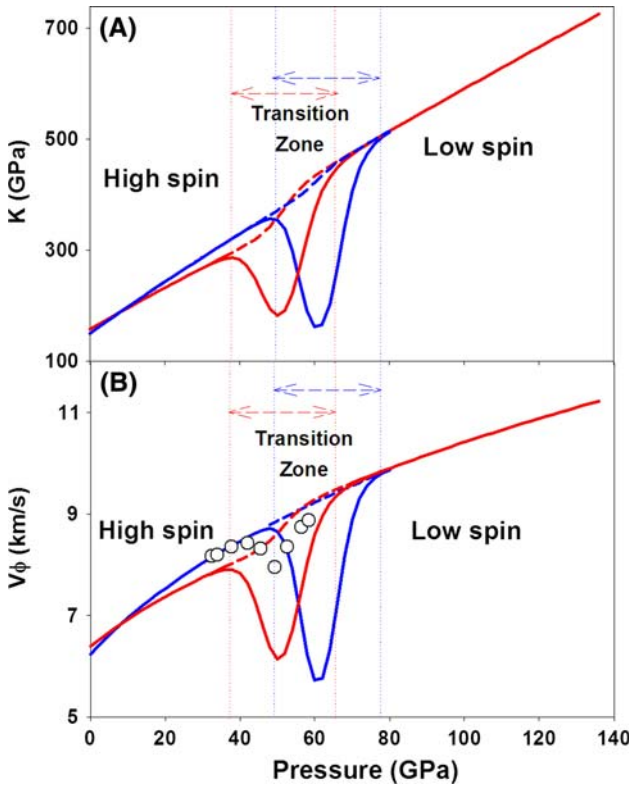


**Fig. 4** Isothermal bulk modulus ($K_T$) (**a**) and bulk sound velocity ($V_\Phi$) (**b**) of ferropericlase $[(Mg_{0.83},Fe_{0.17})O]$ across the spin transition under high pressures. *Red lines*, $K_T$ and $V_\Phi$ derived from data in the Ne pressure medium (Lin et al. 2005); *blue lines*, $K_T$ and $V_\Phi$ derived from this study (non-hydrostatic conditions); *open circles*: $V_\Phi$ of $(Mg_{0.94},Fe_{0.06})O$ by Crowhurst et al. (2008). Blue and red dashed lines represent the average of the separate $K_T$ and $V_\Phi$ of the high-spin and low-spin states. Variation in $K_T$ and $V_\Phi$ within the transition under non-hydrostatic conditions cannot be as well constrained as that in the Ne medium because of the limited available data

## Discussion

### Volume reduction and equation of state (EoS) across the spin transition

Compared with the quasi-hydrostatic compression (Lin et al. 2005), the range of the spin transition is shifted by approximately 20 GPa under non-hydrostatic compression likely as a result of the presence of large differential stress in the sample (Fig. 3). Recent reports of the width of the spin transition in ferropericlase vary significantly from a narrow width in a synchrotron Mössbauer study (Lin et al. 2006a) to a very wide range in a conventional Mössbauer study (Kantor et al. 2006). Our observation of the extension of the spin transition width under non-hydrostatic compression may help explain this discrepancy (Lin et al. 2005, 2006a; Gavriliuk et al. 2006; Kantor et al. 2006; Speziale et al. 2007). Using the EoS of the high-spin ferropericlase from the quasi-hydrostatic study as a reference, the density variation of ferropericlase across the spin transition shows a 3% increase (Fig. 3b).

On the basis of the thermodynamic definition and the finite-strain theory using the third-order Birch–Murnaghan EoS (Birch 1986), we have calculated isothermal bulk modulus ($K_T$) and bulk sound velocity ($V_\Phi$) of ferropericlase $[(Mg_{0.83},Fe_{0.17})O]$ across the spin transition under quasi-hydrostatic condition (in Ne medium; Lin et al. 2005) and non-hydrostatic condition, respectively (Fig. 4). The bulk modulus ($K_T$) is defined thermodynamically as:

$$K_T = -V\frac{dP}{dV} = -\frac{dP}{d\ln V} \quad (1)$$

where $P$ is pressure and $V$ is volume. The bulk sound velocity ($V_\Phi$) is defined as:

$$V_\Phi = \sqrt{\frac{K_S}{\rho}} \quad (2)$$

where $\rho$ is the density and $K_s$ is the adiabatic bulk modulus. The difference between the isothermal and adiabatic bulk moduli was neglected for simplicity. Here the $K_{0T}$ for the high-spin state in the Ne medium alone is 149.7 (±3.7) GPa with a $K_{0T}$' of 4.55 (±0.21), when fitted to the

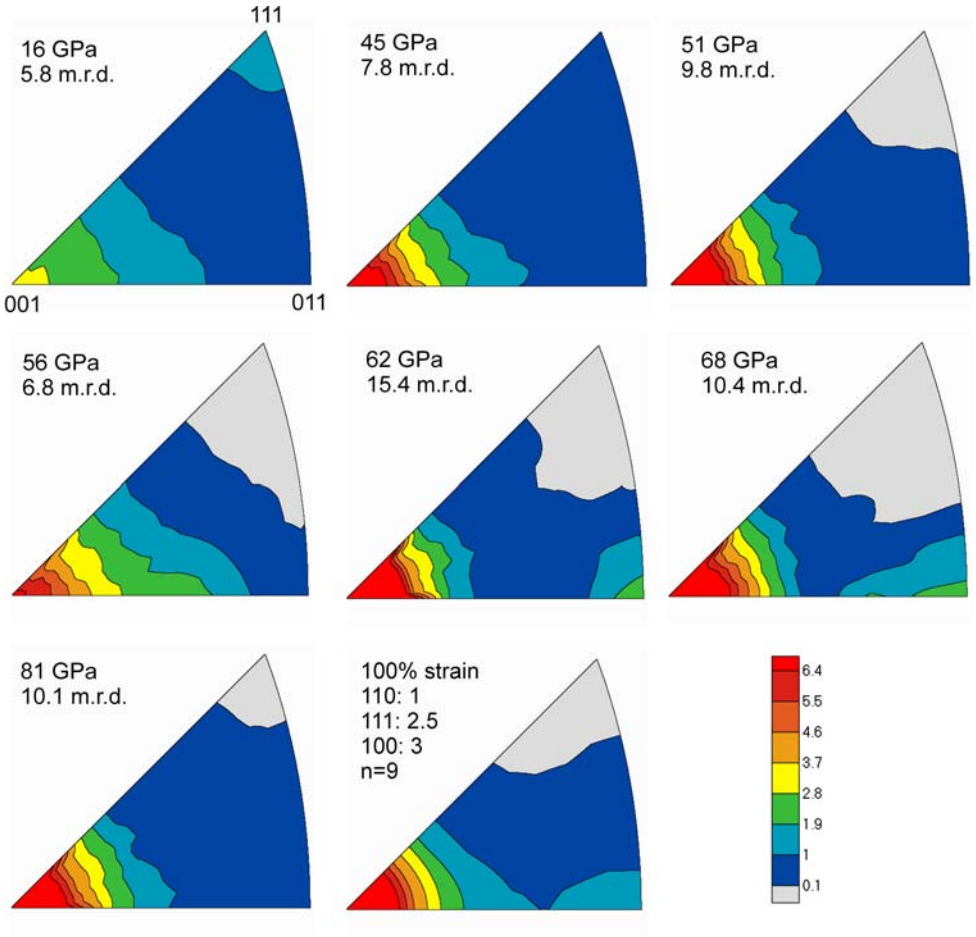


**Fig. 5** Inverse pole figures of the compression direction for $(Mg_{0.83},Fe_{0.17})O$ at high pressures in equal area projection. Pole densities are given in multiples of random distribution (m.r.d.). The experimental inverse pole figures with maximum pole density indicated are followed by a plasticity simulation. In the simulation, 2,000 grains were compressed to 100% equivalent strain in 100 increments. Critical shear stresses were assigned to slip systems corresponding to low temperature deformation, i.e., {1 1 0}<1–10> with 1.0, {1 1 1}<1–10> with 2.5 and {1 0 0}<1–10> with 3.0 and a stress exponent $n = 9$. On the average 5 slip systems were active in each grain. Most deformation occurred on {110} systems (>90%) and much less on {1 1 1} and {1 0 0} systems (<5% each)

experimental data up to 40 GPa based on our current understanding of the spin transition range (Lin et al. 2005; Speziale et al. 2007). The $K_{0T}$ for the low-spin ferropericlase is 205 (±16) GPa with $V_{0LS}/V_{0HS}$ of 0.936 (±0.067) and an assumed $K_{0T}$' of 4, which is derived from fitting the experimental data above 61 GPa (Lin et al. 2005). Because of the limited data under non-hydrostatic condition, the $K_T$ of the low-spin state is assumed the same as that in the Ne medium, and variation in $K_T$ within the transition cannot be as well constrained as that in the Ne medium. A significant reduction in the $K_T$ and $V_\Phi$ occurs within the spin transition (Fig. 4), consistent with a recent high-pressure elasticity study of ferropericlase with 6% FeO (Crowhurst et al. 2008).

## Analyses of the stress and elastic strength of ferropericlase

Using our RXD data and lattice strain theory (Singh et al. 1998; Mao et al. 2008), we have evaluated the $6<Q(hkl)>$ $(=t/G)$ value, the ratio between the differential stress ($t$) and the shear modulus($G$) under constant stress conditions, which represents a proxy for the elastic strength of ferropericlase (Fig. 6) (Singh et al. 1998). The lattice strain theory described above considers the elastic deformation of the sample but does not account for texture and plastic anisotropy (Weidner et al. 2004; Chen et al. 2006). The analysis here assumes that the sample is predominantly subjected to differential stress conditions. The $d$-spacings of the ferropericlase and Mo were obtained from the RXD peaks and plotted a function of the $\psi$ angle between the compression direction and the diffracting plane normal according to the relation (e.g., Singh et al. 1998; Duffy et al. 1999; Shieh et al. 2004; Mao et al. 2008):

$$d_m(hkl) = d_P(hkl)\left[1 + \left(1 - 3\cos^2\psi\right)Q(hkl), \quad (3)$$

where $d_m(hkl)$ is the measured $d$-spacing and $d_P(hkl)$ is the $d$-spacing under the corresponding hydrostatic stress at $\psi$ of 54.7°. $Q(hkl)$ is given by:

$$Q(hkl) = \frac{t}{3}\left(\frac{\alpha}{2G_R(hkl)} + \frac{1-\alpha}{2G_V}\right) \quad (4)$$

where $G_R(hkl)$ and $G_V$ are the aggregate shear modulus for the crystallites contributing the diffracted intensity under the approximations of constant stress (Reuss bound, $G_R$) and constant strain (Voigt bound, $G_V$), respectively, and $t$ is

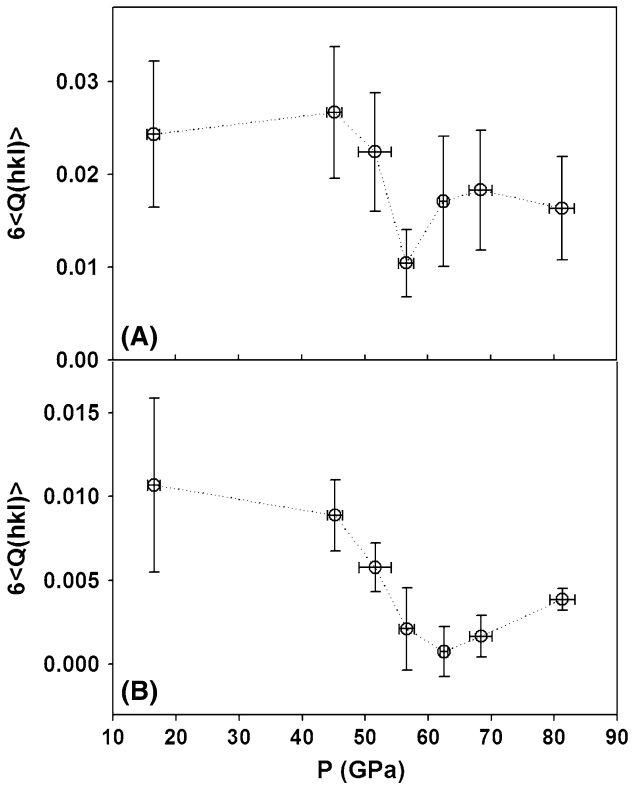


**Fig. 6** Averaged $6<Q(hkl)>$ of (**a**) $(Mg_{0.83},Fe_{0.17})O$ and (**b**) Mo as a function of pressure. The errors on $6<Q(hkl)>$ are calculated from the standard deviation of all $Q(hkl)$ values, which are derived from the $d(hkl)$ and $1–3\cos^2\psi$ relation (Singh et al. 1998). The value of $6<Q(hkl)>$ is reduced significantly in the mixed-spin and low-spin ferropericlase (Fig. 3, 4). The relatively smaller error bar at 55 GPa is likely a result of the volume reduction associated with the spin transition, which results in a relatively more hydrostatic condition

the differential stress, the stress difference between the principle components of the stress field, maximum stress ($\sigma_3$) and minimum stress ($\sigma_1$). The parameter $\alpha$, which varies between 0 and 1, determines the degree of stress and strain continuity across grains in the sample. When constant stress is assumed ($\alpha = 1$), equation (4) is simplified to:

$$6<Q(hkl)> = \frac{t}{G_R(hkl)} \quad (5)$$

where $<Q(hkl)>$ represents the average $Q(hkl)$ value over all observed reflections as determined from equation (3). Previous studies showed that the plastic anisotropy can have an influence on the interpretation of the RXD data using the lattice strain theory (Li et al. 2004; Weidner et al. 2004; Chen et al. 2006; Merkel 2006). That is, the plastic deformation of ferropericlase under uniaxial compression across the spin transition remains to be further investigated and the absolute values of the stress and strength of ferropericlase should be further studied by taking the texture, plasticity, grain size, and total stress/strain into consideration.

The general trend of the derived $6<Q(hkl)>$ values is lower in the mixed-spin states between 51 and 68 GPa and in the low-spin state at 81 GPa than that of the extrapolated high-spin state, although the values exhibit relatively large uncertainties. The high-spin to low-spin transition causes a density increase of about 3% as shown in Fig. 3b which would allow the sample to relax and accommodate to the extrinsic stress field, resulting in a reduced differential stress and $6<Q(hkl)>$ ($=t/G$) value. This phenomenon of the reduced differential stress has been observed across structural transformations from olivine to ringwoodite, ringwoodite to perovskite and periclase, and stishovite to $CaCl_2$-typed structure in $SiO_2$ (Uchida et al. 1995; Shieh et al. 2004).

Examination of the $6<Q(hkl)>$ of Mo shows a reduction at similar pressures, indicating that the reduced differential stress propagated through both Mo and ferropericlase in the sample chamber (Fig. 6b). Knowing that Mo does not undergo any phase transition at such pressures (Hixson and Fritz 1992; Duffy et al. 1999) and that the shear modulus of ferropericlase is reduced within the spin transition pressure range (Crowhurst et al. 2008), the decrease in the $6<Q(hkl)>$ can thus be attributed to the reduced differential stress field through the volume reduction across the spin transition in ferropericlase (Fig. 6). The drastic reduction of the differential stress supported by ferropericlase in the mixed-spin and the low-spin states indicates that the strength of this mineral decreases across the spin transition. Thus the low-spin ferropericlase should exhibit lower strength than what is expected by extrapolation of the high-spin state. The effect of the spin transition on the differential stress of ferropericlase should be less dominant across the wide spin transition zone in the lower mantle (Sturhahn et al. 2005; Tsuchiya et al. 2006; Lin et al. 2007a), making this phenomenon less important in geophysical implications.

## Texture across the spin transition in ferropericlase

Our RXD results show that the {0 0 1} texture is the dominant lattice preferred orientation across the spin transition in ferropericlase at high pressures and room temperature (Fig. 5). Our viscoplastic self-consistent polycrystal plasticity simulations (Lebensohn and Tomé 1993) produce texture patterns with dominant {1 1 0}<1–10> slip that are similar to the experimental observations (Fig. 5) and we infer that this is the main active slip system in the mixed-spin and low-spin states at lower mantle pressures and room temperature. Since the slip system does not change across the spin transition, it is likely that the spin transition would not effect the lattice preferred orientation in ferropericlase over a wide range of pressure–temperature conditions of the lower mantle. Deformation

mechanisms at relevant high temperatures and low stresses of the lower mantle, however, may be different and diffusive mechanisms may play an important role in the deformation (Karato 2008).

## Conclusions

We have carried out in situ radial X-ray diffraction of ferropericlase deformed non-hydrostatically in a diamond cell up to 81 GPa at room temperature in order to understand the texture and deformation of ferropericlase across the spin transition. Compared with recent quasi-hydrostatic studies, an increase in the density of 3% and a decrease in incompressibility has been observed within the spin transition, while the spin transition range is shifted by approximately 20 GPa as a result of the difference in differential stress in the sample. Analyses of our XRD results show that the {0 0 1} texture is the dominant lattice preferred orientation in ferropericlase across the spin transition and in the low-spin state. Our viscoplastic self-consistent polycrystal plasticity simulations indicate that {1 1 0}<1–10> is the dominant slip system across the spin transition in ferropericlase. The $6<Q(hkl)>$ ($=t/G$) values of ferropericlase in the mixed-spin and low-spin states are lower than what is expected by studying high-spin ferropericlase, indicating that the spin transition results in a reduced differential stress as a result of the volume reduction.

Earlier measurements on the rheological properties of ferropericlase under high pressures and/or high temperatures have been used to constrain the deformation and fabric development of ferropericlase in the lower mantle; however, these studies were limited to the high-spin ferropericlase at pressure–temperature conditions lower than that of the lower mantle (e.g., Stretton et al. 2001; Yamazaki and Karato 2002; Heidelbach et al. 2003; Long et al. 2006; Tommaseo et al. 2006). Our results extend the pressure range across the spin transition, and show that the differential stress and elastic strength of ferropericlase are significantly reduced within the spin transition and in the low-spin ferropericlase. The influence of the spin transition on the relaxation of the differential stress in ferropericlase is expected to be less dominant across the spin transition zone in the lower mantle. Future studies on the deformation mechanisms across the spin transition under relevant lower-mantle pressure–temperature-stress conditions are needed to further enhance our understanding of the lower mantle rheology.

**Acknowledgments** We acknowledge J. Hu, NSLS, and COMPRES for the use of the X17C synchrotron facilities. We thank J. Hu for helping with the data collection and J. Kung for providing the ferropericlase sample. We acknowledge D. Weidner, S.-i. Karato, and S. Merkel for constructive discussions. J.F.L. acknowledges financial support from NSF Earth Sciences (EAR-0838221) and Carnegie/DOE Alliance Center (CDAC) at Carnegie Institution of Washington. H.R.W. is appreciative for support from NSF (EAR 0836402), DOE-CDAC and LLNL-IGPP.

## References

Badro J, Fiquet G, Guyot F, Rueff JP, Struzhkin VV, Vankó G, Monaco G (2003) Iron partitioning in Earth's mantle: toward a deep lower mantle discontinuity. Science 300:789–791. doi:10.1126/science.1081311

Birch F (1986) Equation of state and thermodynamic parameters of NaCl to 300 kbar in the high-temperature domain. J Geophys Res 91:4949–4954. doi:10.1029/JB091iB05p04949

Chen J, Li L, Yu T, Long H, Weidner D, Wang L, Vaughan M (2006) Do Reuss and Voigt bounds really bound in high-pressure rheology experiments? J Phys Condens Matter 18:S1049–S1059. doi:10.1088/0953-8984/18/25/S11

Crowhurst J, Brown JM, Goncharov A, Jacobsen SD (2008) Elasticity of (Mg,Fe)O through the spin transition of iron in the lower mantle. Science 319:451–453. doi:10.1126/science.1149606

Duffy TS, Shen G, Shu J, Mao HK, Hemley RJ, Singh AK (1999) Elasticity, shear strength, and equation of state of molybdenum and gold from X-ray diffraction under nonhydrostatic compression to 24 GPa. J Appl Phys 86:6729–6736. doi:10.1063/1.371723

Fei Y, Zhang L, Corgne, Watson H, Ricolleau A, Meng Y, Prakapenka V (2007) Spin transition and equations of state of (Mg,Fe)O solid solutions. Geophys Res Lett 34:L17307. doi:10.1029/2007GL030712

Gavriliuk AG, Lin JF, Lyubutin IS, Struzhkin VV (2006) Optimization of the conditions of synchrotron Mössbauer experiment for studying electron transitions at high pressures by the example of (Mg,Fe)O magnesiowüstite. J Exp Theor Phys Lett 84:161–166. doi:10.1134/S0021364006150136

Goncharov AF, Struzhkin VV, Jacobsen SD (2006) Reduced radiative conductivity of low-spin (Mg,Fe)O in the lower mantle. Science 312:1205–1208. doi:10.1126/science.1125622

Heidelbach F, Stretton I, Langenhorst F, Mackwell S (2003) Fabric evolution during high shear–strain deformation of magnesiowüstite. J Geophys Res B 108:2154. doi:10.1029/2001JB001632

Hixson RS, Fritz JN (1992) Shock compression of tungsten and molybdenum. J Appl Phys 71:1721–1728. doi:10.1063/1.351203

Kantor IY, Dubrovinsky LS, McCammon CA (2006) Spin crossover in (Mg,Fe)O: a Mössbauer effect study with an alternative interpretation of X-ray emission spectroscopy data. Phys Rev B 73:100101. doi:10.1103/PhysRevB.73.100101

Karato S-I (1998) Seismic anisotropy in the deep mantle and the geometry of mantle convection. Pure Appl Geophys 151:565–587. doi:10.1007/s000240050130

Karato S-i (2008) Deformation of earth materials. Cambridge University Press, New York, p 463

Keppler H, Kantor I, Dubrovinsky LS (2007) Optical absorption spectra of ferropericlase to 84 GPa. Am Min 92:433–436. doi:10.2138/am.2007.2454

Lebensohn RA, Tomé CN (1993) A self-consistent anisotropic approach for the simulation of plastic deformation and texture development of polycrystals–application to zirconium alloys. Acta Metall Mater 41:2611–2624. doi:10.1016/0956-7151(93)90130-K

Li L, Weidner DJ, Chen J, Vaughan MT, Davis M, Durham WB (2004) X-ray strain analysis at high pressure: effect of plastic

deformation in MgO. J Appl Phys 95:8357–8365. doi:10.1063/1.1738532
Lin JF, Tsuchiya T (2008) Spin transition of iron in the Earth's lower mantle. Phys Earth Planet Inter 170:248–259. doi:10.1016/j.pepi.2008.01.005
Lin JF, Struzhkin VV, Jacobsen SD, Hu M, Chow P, Kung J, Liu H, Mao HK, Hemley RJ (2005) Spin transition of iron in magnesiowüstite in Earth's lower mantle. Nature 436:377–380. doi:10.1038/nature03825
Lin JF, Gavriliuk AG, Struzhkin VV, Jacobsen SD, Sturhahn W, Hu M, Chow P, Yoo CS (2006a) Pressure-induced electronic spin transition of iron in magnesiowüstite-(Mg,Fe)O. Phys Rev B 73:113107. doi:10.1103/PhysRevB.73.113107
Lin JF, Jacobsen SD, Sturhahn W, Jackson JM, Zhao J, Yoo CS (2006b) Sound velocities of ferropericlase in Earth's lower mantle. Geophys Res Lett 33:L22304. doi:10.1029/2006GL028099
Lin JF, Vankó G, Jacobsen SD, Iota V, Struzhkin VV, Prakapenka VB, Kuznetsov A, Yoo CS (2007a) Spin transition zone in Earth's lower mantle. Science 317:1740–1743. doi:10.1126/science.1144997
Lin JF, Weir ST, Jackson DD, Evans WJ, Yoo CS (2007b) Electrical conductivity of the low-spin ferropericlase in the Earth's lower mantle. Geophys Res Lett 34:L16305. doi:10.1029/2007GL030523
Lin JF, Watson HC, Vankó G, Alp EE, Prakapenka VB, Dera P, Struzhkin VV, Kubo A, Zhao J, McCammon C, Evans WJ (2008) Intermediate-spin ferrous iron in lowermost mantle post-perovskite and perovskite. Nat Geosci 1:688–691. doi:10.1038/ngeo310
Long MD, Xiao X, Jiang Z, Evans B, S-i Karato (2006) Lattice preferred orientation in deformed polycrystalline (Mg,Fe)O and implications for seismic anisotropy in D". Phys Earth Planet Int 156:75–88. doi:10.1016/j.pepi.2006.02.006
Lutterotti L, Matthies S, Wenk H-R, Schultz AJ, Richardson JW (1997) Combined texture and structure analysis of deformed limestone from time-of-flight neutron diffraction spectra. J Appl Phys 81:594–600
Mao WL, Struzhkin VV, Baron AQR, Tsutsui S, Tommaseo CE, Wenk HR, Hu MY, Chow P, Sturhahn W, Shu J, Hemley RJ, Heinz DL, Mao HK (2008) Experimental determination of the elasticity of iron at high pressure. J Geophys Res 113:B09213
McCammon C, Kantor I, Narygina O, Rouquette J, Ponkratz U, Sergueev I, Mezouar M, Prakapenka V, Dubrovinsky L (2008) Stable intermediate-spin ferrous iron in lower-mantle perovskite. Nat Geosci 1:684–687. doi:10.1038/ngeo309
McNamara AK, van Keken PE, Karato S-i (2002) Development of anisotropic structure in the Earth's lower mantle by solid-state convection. Nature 416:310–314. doi:10.1038/416310a
Merkel S (2006) X-ray diffraction evaluation of stress in high pressure deformation experiments. J Phys Condens Matter 18:S949–S962. doi:10.1088/0953-8984/18/25/S03
Merkel S, Wenk HR, Shu J, Shen G, Gillet P, Mao HK, Hemley RJ (2002) Deformation of polycrystalline MgO at pressures of the lower mantle. J Geophys Res 107:2271. doi:10.1029/2001JB000920
Persson K, Bengtson A, Ceder G, Morgan D (2006) Ab initio study of the composition dependence of the pressure-induced spin transition in the $(Mg_{1-x},Fe_x)O$ system. Geophys Res Lett 33:L16306. doi:10.1029/2006GL026621
Ringwood AE (1982) Phase transformations and differentiation in subducted lithosphere: implications for mantle dynamics basalt petrogenesis and crustal evolution. J Geol 90:611–642
Shannon RD, Prewitt CT (1969) Effective ionic radii in oxides and fluorides. Acta Crystallogr B 25:925–946. doi:10.1107/S0567740869003220
Shieh SR, Duffy TS, Li B (2004) Strength and elasticity of $SiO_2$ across the stishovite-$CaCl_2$-type structural phase boundary. Phys Rev Lett 89:255507. doi:10.1103/PhysRevLett.89.255507
Singh AK, Balasingh C, Mao HK, Hemley RJ, Shu J (1998) Analysis of lattice strains measured under non-hydrostatic pressure. J Appl Phys 83:7567–7575. doi:10.1063/1.367872
Speziale S, Zha C-S, Duffy TS, Hemley RJ, Mao HK (2001) Quasi-hydrostatic compression of magnesium oxide to 52 GPa: implications for the pressure–volume–temperature equation of state. J Geophys Res 106:515–528. doi:10.1029/2000JB900318
Speziale S, Lee VE, Clark SM, Lin JF, Pasternak MP, Jeanloz R (2007) Effects of Fe spin transition on the elasticity of (Mg,Fe)O magnesiowüstites and implications for the seismological properties of the Earth's lower mantle. J Geophys Res 112:B10212. doi:10.1029/2006JB004730
Stretton I, Heidelbach F, Mackwell SJ, Langenhorst F (2001) Dislocation creep of magnesiowüstite ($Mg_{0.8}Fe_{0.2}O$). Earth Planet Sci Lett 194:229–240. doi:10.1016/S0012-821X(01)00533-7
Sturhahn W, Jackson JM, Lin JF (2005) The spin state of iron in Earth's lower mantle minerals. Geophys Res Lett 32:L12307. doi:10.1029/2005GL022802
Tommaseo CE, Devine J, Merkel S, Speziale S, Wenk H-R (2006) Texture development and elastic stresses in magnesiowüstite at high pressure. Phys Chem Miner 33:84–97. doi:10.1007/s00269-005-0054-x
Tsuchiya T, Wentzcovitch RM, da Silva CRS, de Gironcoli S (2006) Spin transition in magnesiowüstite in Earth's lower mantle. Phys Rev Lett 96:198501. doi:10.1103/PhysRevLett.96.198501
Uchida T, Funamori N, Ohtani T, Yagi T (1995) Differential stress of MgO and $Mg_2SiO_4$ under uniaxial stress field: variation with pressure, temperature, and phase transition. High-pressure Sci Technol, AIRAPT-15 5:183–185
Weaver CW, Paterson MS (1969) Deformation of cube-oriented MgO crystals under pressure. J Am Ceram Soc 52:293–302. doi:10.1111/j.1151-2916.1969.tb11929.x
Weidner DJ, Li L, Davis M, Chen J (2004) Effect of plasticity on elastic modulus measurements. Geophys Res Lett 31:1–4. doi:10.1029/2003GL019090
Wenk H-R, Matthies S, Donovan J, Chateigner D (1998) Beartex: a Windows-based program system for quantitative texture analysis. J Appl Cryst 31:262–269. doi:10.1107/S002188989700811X
Wenk H-R, Speziale S, McNamara AK, Garnero EJ (2006) Modeling lower mantle anisotropy development in a subducting slab. Earth Planet Sci Lett 245:302–314. doi:10.1016/j.epsl.2006.02.028
Yamazaki D, Karato S-i (2002) Fabric development in (Mg,Fe)O during large strain, shear deformation: implications for seismic anisotropy in Earth's lower mantle. Phys Earth Planet Int 131:251–267. doi:10.1016/S0031-9201(02)00037-7